Evaluation of the Effectiveness of Biomineralization Technology in Repairing the Strength of Damaged Fiber-Reinforced LWAC

How-Ji Chen , Tsung-Kai Chen , Chao-Wei Tang * , And Han-Wen Chang

Posted Date: 20 November 2023

doi: 10.20944/preprints202311.1233.v1

Keywords: biomineralization; lightweight aggregate concrete; compressive strength; bond strength

Article

Evaluation of the Effectiveness of Biomineralization Technology in Repairing the Strength of Damaged Fiber-Reinforced LWAC

How-Ji Chen [1], Tsung-Kai Chen [1], Chao-Wei Tang [2,3,4,*] and Han-Wen Chang [1]

[1] Department of Civil Engineering, National Chung-Hsing University, 145 Xingda Rd., South District, Taichung City 40227, Taiwan; hojichen@dragon.nchu.edu.tw (H.-J.C.); ru9378@gmail.com (T.-K.C.); awiuyg58799@yahoo.com.tw (H.-W.C.)

[2] Department of Civil Engineering and Geomatics, Cheng Shiu University, No. 840, Chengching Rd., Niaosong District, Kaohsiung 83347, Taiwan

[3] Center for Environmental Toxin and Emerging-Contaminant Research, Cheng Shiu University, No. 840, Chengching Rd., Niaosong District, Kaohsiung 83347, Taiwan

[4] Super Micro Mass Research and Technology Center, Cheng Shiu University, No. 840, Chengching Rd., Niaosong District, Kaohsiung 83347, Taiwan

* Correspondence: tangcw@gcloud.csu.edu.tw; Tel.: +886-7-735-8800

Abstract: Concrete cracks and local damage can affect the bond performance between concrete and steel bars, thereby reducing the durability of reinforced concrete structures. Compared with general concrete crack repair methods, biomineralization repair not only has effective bonding capabilities but is also particularly environmentally friendly. In view of this, this study aimed to apply biomineralization technology to repair damaged fiber-reinforced lightweight aggregate concrete (LWAC). Two groups of LWAC specimens were prepared. The control group used lightweight aggregates (LWAs) without bacterial spores and nutrient sources, and the experimental group used LWAs containing bacterial spores and nutrient sources. These specimens were first subjected to compression tests and pull-out tests, respectively, and thus were damaged. After the damaged specimen healed itself in different ways for 28 days, secondary compression and pull-out tests were conducted. The self-healing method of the control group involved placing the specimens in an incubator. The experimental group was further divided into experimental group I and experimental group II. The self-healing method of experimental group I was the same as that of the control group. The self-healing method of experimental group II involved soaking the specimen in a mixed solution of urea and calcium acetate for two days, and then taking it out and placing it in an incubator for two days, with a cycle of four days. The test results showed that, compared with the control group specimens, the relative bond strength ratio of the experimental group II specimens increased by 17.9%. Moreover, the EDS and XRD analysis results confirmed that the precipitate formed at the crack was calcium carbonate, which improved the compressive strength and bond strength after self-healing. This indicates that the biomineralization maintenance method used in experimental group II is more effective.

Keywords: biomineralization; lightweight aggregate concrete; compressive strength; bond strength

1. Introduction

Lightweight aggregate concrete (LWAC) generally refers to concrete produced by replacing normal-weight aggregates with lightweight aggregates (LWAs) with a smaller unit weight or specific gravity [1]. According to the difference in unit weight and strength, ACI divides lightweight concrete into three grades: low-density concrete, medium-strength concrete, and structural concrete, as shown in Figure 1 [2]. The use of structural LWAC can not only reduce the weight of the structure by more than 20%, but also effectively reduce the seismic load of the building structure [3–5]. However, compared with normal-weight concrete (NWC) of the same compressive strength, LWAC exhibits some disadvantages, such as higher brittleness and lower mechanical properties [6,7]. In view of this, scholars believe that using fibers in LWAC is a suitable improvement solution to solve such problems

Preprints (www.preprints.org) | NOT PEER-REVIEWED | Posted: 20 November 2023 doi:10.20944/preprints202311.1233.v1

[8–10]. In the past two decades, with the continuous improvement in artificial LWA production technology and the use of fibers, the mechanical properties of fiber-reinforced LWAC have been significantly improved. As a result, the application of LWAC in structural concrete is more common [11,12].

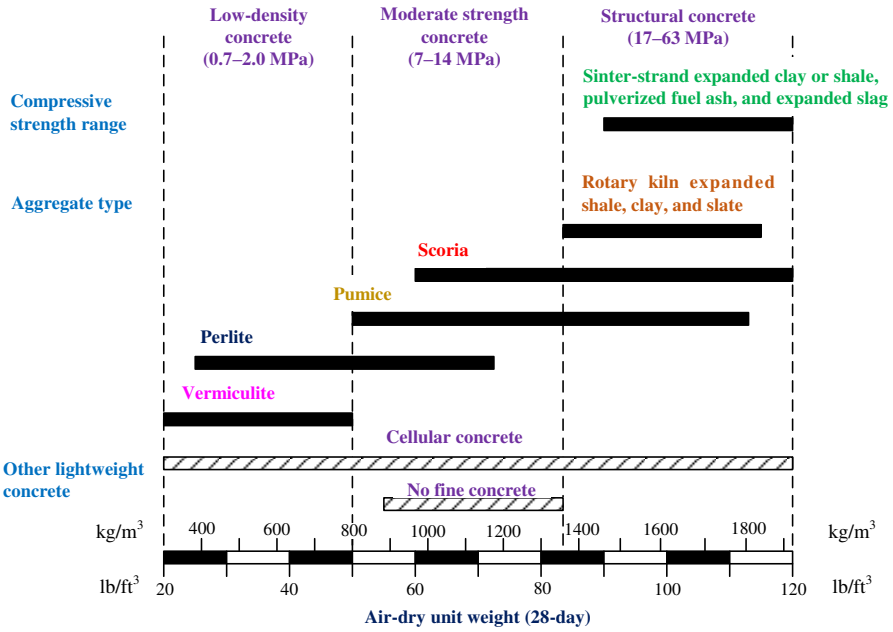

Figure 1. Unit weight and classification of lightweight concrete.

In general, for reinforced concrete (RC) members, a sufficient bond between the steel bars and the surrounding concrete is a prerequisite for the synergy between the two materials. Similarly, the bond slip characteristics between steel bars and LWAC are also the main mechanism to enhance the load-bearing capacity and coordinated deformation of LWAC components and can be used to analyze the mechanical properties of its key parts [13–15]. The ACI 408-03 specification [16] states that efficient and reliable load transfer from steel reinforcement to surrounding concrete is necessary for the optimal design of RC structures. According to the definition of ACI 318 [17], bond stress is the shear stress transmitted along the steel–concrete interface. For deformed steel bars, the ability of this interface to transfer stress between the two materials consists primarily of three resistance mechanisms: (1) chemical adhesion between the steel and concrete; (2) friction between the two surfaces; and (3) the mechanical interlock of the ribs against the concrete [16,18].

Due to the lower strength of LWA, many studies have pointed out that, at the same compressive strength level, the bond strength between LWAC and steel bars is worse than that between NWC and steel bars [19,20]. For this reason, ACI 318-19 recommends a development length correction factor of 1.3 for steel bars to reflect the lower mechanical strength of LWAC compared to NWC of the same compressive strength [17]. However, many studies show different results [4,21–23]. Mo et al. [21] showed that the relatively high cementitious material content and the excellent interlocking effect of LWA jointly improve the bond strength of LWAC. They pointed out that the maximum bond stress of a well-constrained LWAC is about $3.5\sqrt{f_c'}$, which is larger than the value of $2.5\sqrt{f_c'}$ suggested by the CEB-FIP standard [24].

The bond stress between steel bars and concrete is related to several parameters, such as the compressive strength of the concrete, the roughness and/or irregularity of the steel bar surface, the diameter of the steel bars, and the type and configuration of the ribs. Shima et al. [25] proposed that the bond–slip relationship can be expressed in terms of bond stress, slip, and rebar strain. Kankam [26] established the relationship between bond stress, steel bar stress, and slip based on experimental analysis. In the study of the bond–slip behavior between steel bars and concrete, the bond stress versus slip curve is the most-used expression. The bond stress–slip curve shows the bond stress and slip at different load levels, the maximum bond stress, and the slip at the maximum bond stress.

Preprints (www.preprints.org) | NOT PEER-REVIEWED | Posted: 20 November 2023 doi:10.20944/preprints202311.1233.v1

Eligehausen et al. [27] proposed the bond–slip constitutive relationship of deformed steel bars under monotonic and cyclic loads. Filippou et al. [28] established an analytical model describing the hysteretic behavior of reinforced concrete beam–column joints. Therefore, this model is collectively referred to as the Eligehausen–Filippou model. This model was also adopted by the CEB-FIP Model Code 1990 [29] and 2010 [24], which includes four different branches: the curve rising stage; the constant maximum stage; the linear decreasing stage; and the constant friction adhesive stress stage, as Figure 2 shows. In the case of pull-out failure, the bond stress (τ) between concrete and steel bars as a function of relative displacement (s) can be calculated using the following equation:

$$\tau = \tau_u (s/s_1)^{\alpha} \text{ for } 0 \le s \le s_1 \quad (1)$$

$$\tau = \tau_u \text{ for } s_1 < s \le s_2 \quad (2)$$

$$\tau = \tau_u - (\tau_u - \tau_f)\left(\frac{s - s_2}{s_3 - s_2}\right) \text{ for } s_2 < s \le s_3 \quad (3)$$

$$\tau = \tau_f \text{ for } s_3 < s \quad (4)$$

where τ_u and τ_f are the peak bond stress and the residual bond stress, respectively; s_1, s_2, and s_3 are the slip at the start of peak bond stress, slip at the end of peak bond stress, and slip at the start of residual bond stress, respectively; and α is a curve-fitting parameter.

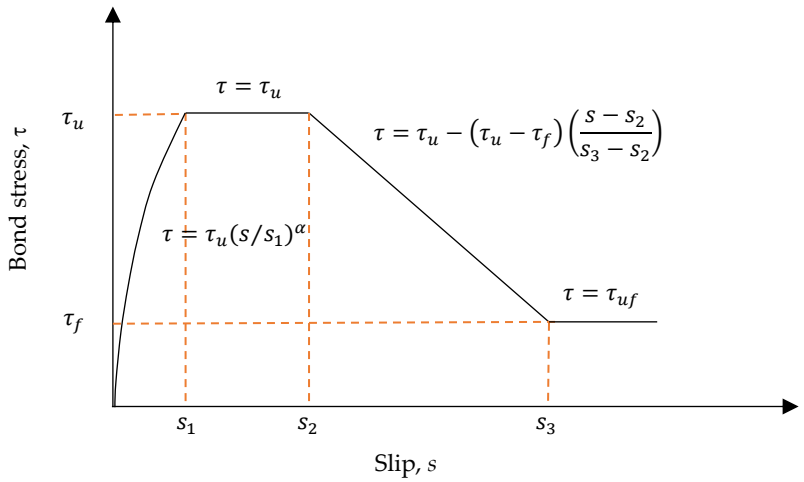

Figure 2. Particle size distribution curve of fine aggregate.

Due to the complex mechanisms of bond stress and slip, piecewise equations based on experimental results are generally used to express the bond–slip relationship [25,26,29–31]. However, due to the dispersion of concrete materials and different testing conditions, the key points of the bond–slip relationship proposed by different researchers are quite different [32–34]. For example, the bond strength is mainly described by $\alpha(f_c')^{\beta}$, while the variation ranges of α and β are 2.5 to 3.5 and 0.5 to 1, respectively. In addition, the key points, such as the peak bond stress and residual bond stress, of LWAC are not like those of NWC, as shown in Table 1.

Table 1. Parameter values for the prediction models for the bond stress–slip relationship.

Parameter	Model Code 2010 (2010)		Harajli et al. (1995)
	Confined NWC	Confined LWAC	Concrete
s_1	1.0 mm	1.0 mm	0.15 Distance bet. ribs

Preprints (www.preprints.org) | NOT PEER-REVIEWED | Posted: 20 November 2023 doi:10.20944/preprints202311.1233.v1

s_2	3.0 mm	2.0 mm	0.35 Distance bet. ribs
s_3	Clear rib spacing	Clear rib spacing	Distance bet. ribs
α	0.4	0.35	0.3
τ_u	$2.5\sqrt{f_c'}$	$0.6(f_c')^{0.82}$	$2.57\sqrt{f_c'}$
τ_f	$0.4\tau_u$	$0.15\tau_u$	$0.9\sqrt{f_c'}$

Under the action of load and environment, concrete will deform [10]. These deformations often lead to cracking or localized damage to the concrete, adversely affecting its impermeability, resistance to chloride ion attack, and resistance to carbonization. Cracks or local damage to RC components can easily lead to the loss of the bond force between steel bars and concrete [35]. Many different repair methods have been developed to address the factors that cause concrete cracks to form. However, the materials currently used for repairing concrete cracks are mostly epoxy resin systems, acrylic resins, or silicone polymers [36,37], which are not friendly to the environment. In view of this, ecologically sound and sustainable biological system restoration technology has become a feasible alternative [38–49]. Biomineralization is a widely occurring effect in nature and is defined as the process by which organisms produce minerals through metabolic activities related to interactions with the environment [38]. Concrete self-healing technology based on biomineralization mainly refers to the use of microbial metabolism to generate insoluble compounds to achieve the self-healing effect of concrete materials. Microbiologically induced calcium carbonate precipitation (MICP) is ubiquitous in nature; that is, specific microorganisms can react with their own life activities to mineralize and form calcium carbonate crystals ($CaCO_3$), and deposit them on the surface of bacterial cells [39]. These calcium carbonate crystals exhibit high strength and stability, filling the gaps between particles and binding them together as a cementing material. When bacteria are added directly to concrete, the highly alkaline environment can easily lead to the death of such unprotected bacteria [40]. Therefore, appropriate bacterial carriers must be selected [41]. At present, carriers are mainly divided into natural carrier materials and synthetic carrier materials [42]. Jonkes et al. [43] studied the ability of alkali-resistant spore-forming bacteria to repair concrete cracks and confirmed that the potential application of bacterial spores as self-healing agents seems promising. MICP is a natural stone with excellent environmental protection and durability properties and shows excellent compatibility with cement-based materials. It can strengthen or repair cement-based materials to improve their pore structure and repair concrete cracks. Compared with physical strengthening and chemical strengthening methods, MICP technology is environmentally friendly and has obvious advantages and broad prospects for repairing concrete cracks.

Cracks or local damage to concrete often lead to a decrease in its mechanical properties, which, in turn, affects its bond behavior with steel bars, ultimately resulting in a decrease in the durability of reinforced concrete structures. There are few studies on the bond behavior between steel bars and the self-healing LWAC matrix. In view of this, the purpose of this study is to apply biomineralization technology to repair the strength of damaged fiber-reinforced LWAC. In this study, fiber-reinforced LWAC specimens were prepared in the control group and the experimental group. The fiber-reinforced LWAC in the experimental group used LWAs as bacterial carriers to increase the survival probability of bacteria. The fiber-reinforced LWAC in the control group did not contain bacterial spores. For each group of concrete specimens, planned tests included compressive strength and pull-out tests. Furthermore, the precipitates formed at the cracks of the biomineralized repaired LWAC samples were analyzed using a crack width meter, a field emission scanning electron microscope, an X-ray energy spectrometer, and an X-ray diffractometer.

 doi:10.20944/preprints202311.1233.v1

2. Experimental Procedure

2.1. Experimental Program

When the two groups of LWAC specimens were cured to 28 days of age, compressive strength and pull-out tests were conducted. Then, the two groups of specimens damaged by the tests were subjected to different curing methods. The curing method of the control group was to place the specimens in an incubator for self-healing. The experimental group was further divided into experimental group I and experimental group II. The curing method of experimental group I was the same as that of the control group. The curing method of experimental group II was to immerse the specimen in a mixed solution of urea and calcium acetate for two days, and then take it out and put it in an incubator for two days, with one cycle lasting four days. After reaching the planned age, the specimens were subjected to secondary compressive strength and pull-out tests. The crack healing was also observed, and the composition of the repair compound was identified. The experimental plan of this study is shown in Table 2. The test items include a compressive strength test, a pull-out test, crack repair observation, field emission scanning electron microscope (FESEM) observation, an X-ray energy spectrometer (EDS) analysis, and an X-ray diffraction (XRD) analysis. The test parameters include curing methods and self-healing age.

Table 2. Test items and test parameters.

Test Items	Test Parameters	
	Curing method	Self-healing age (day)
Compressive strength test	Incubator, cyclical treatment	0
Pull-out test	Incubator, cyclical treatment	0
Secondary compressive strength test	Incubator, cyclical treatment	28
Secondary pull-out test	Incubator, cyclical treatment	28
Observation of crack repair	Incubator, cyclical treatment	0, 7, 14
FESEM, EDS, and XRD analysis	Incubator, cyclical treatment	0, 28

2.2. Materials

The materials used in this research were as follows:

- *Sporosarcina pasteurii* is a Gram-positive aerobic bacterium. It was provided by Moji Technology Co., Ltd.
- Calcium lactate was used as a nutrient source for *pasteurii*. It was purchased from Huacheng Industrial Raw Materials Co., Ltd.
- Yeast extract (YE) is the concentrated content of yeast cells. It can be used as a nutritional supplement. It contains a large amount of protein, amino acids, and the vitamin B group. It was purchased from Huacheng Industrial Raw Materials Co., Ltd.
- Calcium acetate was used as a supplementary source of external calcium ions during the maintenance of the specimens. It was purchased from Huacheng Industrial Raw Materials Co., Ltd.
- Urea is an organic compound composed of carbon, nitrogen, oxygen, and hydrogen, and was purchased from Huacheng Industrial Raw Materials Co., Ltd.
- The cement was a locally produced Type I Portland cement with a specific gravity of 3.15 and a fineness of 3550 cm^2/g; its chemical composition is shown in Table 3.

Preprints (www.preprints.org) | NOT PEER-REVIEWED | Posted: 20 November 2023 doi:10.20944/preprints202311.1233.v1

- The water was general tap water, which is in line with the general quality requirements of concrete mixing water.
- The fine aggregate was a natural river sand with an FM value of 2.7 and a 24-hour water absorption rate of 1.15%. Its particle size distribution curve is shown in Figure 3.
- The LWA was artificial aggregate, as shown in Figure 4. Its basic properties are listed in Table 4.
- The original maximum particle size of the LWA was 3/4 inches; the crushed maximum particle size of the LWA was 3/8 inches; the particle density was 1.57 g/cm^3; the dry unit weight was 927 kg/m^3; the specific gravity was 2.65; the water absorption was 6%; and the crushing strength was 12.67 MPa.
- The superplasticizer was a product of the Taiwan Sika Company; its chemical composition was water-modified polycarboxylate, and it met the requirements of C494/C494M-17 [50] Type F.
- The fibers were the products of Guli Li Co., Ltd. We used short micro-steel fibers (according to ASTM A820/A820M-06 [51]) and polypropylene fibers, as shown in Figure 5. The basic properties of the two fibers are shown in Table 5.
- For the longitudinal main reinforcement of the pull-out, #6 rebar was used. Its physical and mechanical properties are shown in Table 6.

Table 3. Chemical compositions of the cementitious materials.

Chemical Composition (%)	Cement
Silicon dioxide, SiO_2	20.48
Aluminum oxide, Al_2O_3	5.93
Iron oxide, Fe_2O_3	3.39
Calcium oxide, CaO	65.50
Magnesium oxide, MgO	2.06
Sulfur trioxide, SO_3	2.39
Free calcium oxide, f-CaO	0.78
Loss on ignition, LOI	0.76
Tricalcium silicate, C_3S	59.50
Dicalcium silicate, C_2S	13.83
Tricalcium aluminate, C_3A	9.98

Table 4. Basic properties of LWAs.

Items	State of LWAs	
	With Bacterial Spores	Without Bacterial Spores
Dry unit weight (kg/m^3)	622.1	618.8
Porosity (%)	47.53	45.22
Bulk specific gravity	1.188	1.172
Apparent gravity	1.246	1.233
1-hour water absorption rate (%)	8.6	11.4
24-hour water absorption rate (%)	10.3	13.3
Crushing strength (MPa)	4.3	4.4

Table 5. Basic properties of fibers.

Fiber Type	Length (mm)	Diameter (mm)	Density (g/cm^3)	Elastic Modulus (GPa)	Tensile Strength (MPa)	Melting Point (°C)
Steel fibers	13	0.2	7.8	200	2000	-
Polypropylene fibers	12	0.05	0.9	-	300	165

Preprints (www.preprints.org) | NOT PEER-REVIEWED | Posted: 20 November 2023 doi:10.20944/preprints202311.1233.v1

Table 6. Basic properties of rebar.

Nominal Dia. (mm)	Rib Distance (mm)	Rib Width (mm)	Rib Height (mm)	Yield Strength (MPa)	Tensile Strength (MPa)
19.1	11.1	4.0	1.0	457	658

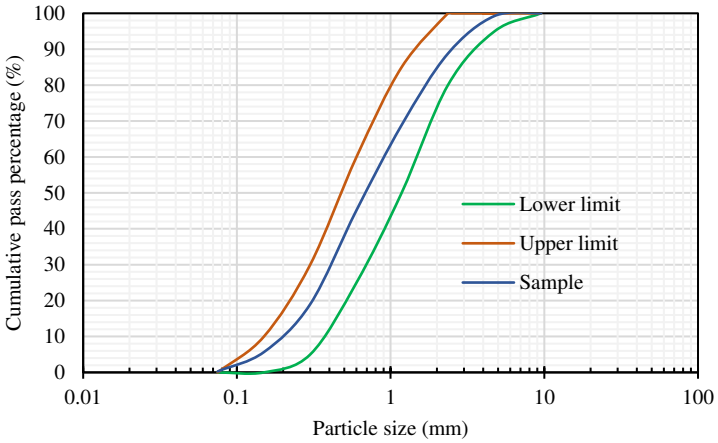

Figure 3. Particle size distribution curve of fine aggregate.

Figure 4. Appearance of expanded shale LWAs.

(**a**) (**b**)

Figure 5. Fibers used in this study: (**a**) short micro-steel fibers, and (**b**) polypropylene fibers.

2.3. Strain Implantation

Details of the strain culture and sporulation can be found in the author's previously published articles [44,49]. The LWAs in the experimental group were used as strain carriers. The steps for implanting the strains into the LWAs were as follows:

(a) The LWAs were washed with clean water. Afterwards, the LWAs were dried to a dry state. Then, the LWAs were immersed in a nutrient source solution containing calcium lactate (80 g/L) and yeast extract (1 g/L) for 60 min. The samples were stirred every 10 minutes, as shown in Figure 6.

(b) The soaked LWA was taken out and drained. Then, the drained LWA was evenly spread on the iron plate and placed in an oven at a constant temperature of 37 °C to dry for 5 days, as shown in Figure 7.

 doi:10.20944/preprints202311.1233.v1

(c) The previous two steps were repeated once.
(d) The nutrient-containing LWAs were immersed in the bacterial spore solution for 60 minutes, during which the pump continued to run and stir every 10 minutes, as shown in Figure 8.
(e) After the LWAs were soaked, they were taken out and drained, spread on an iron plate, and then placed in an oven at 37 °C to dry for five days.

Figure 6. Image of LWAs immersed in a nutrient solution.

(a) **(b)**

Figure 7. Processing of LWAs after immersion in a nutrient solution: (a) draining and (b) drying.

Figure 8. Image of LWAs immersed in a bacterial solution.

2.4. Mix Proportions of LWAC

Two groups of LWAC were prepared for this study. The control group used LWAs without bacterial strains implanted, while the experimental group used LWAs implanted with bacterial strains. The 28-day design compressive strength was 35 MPa for both groups of LWAC, and their required compressive strength was 45 MPa for both groups. According to ACI 211.2, considering the workability, strength, and durability of the two groups of LWAC, the dosage of each material was determined through trial mixing, as shown in Table 7. When mixing the LWAC mixture, the saturated-surface dry fine aggregate and cement were placed into the mixing drum and dry-mixed thoroughly for about one minute at a speed of 140 ± 5 rpm. At the same time, the steel fibers and polypropylene fibers were sprinkled evenly into the mixing drum by hand, and dry-mixed

Preprints (www.preprints.org) | NOT PEER-REVIEWED | Posted: 20 November 2023 doi:10.20944/preprints202311.1233.v1

thoroughly for three minutes until they were uniform. Afterwards, the dry LWAs were poured into the mixing drum and stirred at a speed of 285 ± 10 rpm for about one minute. Then, the pre-mixed water and superplasticizer were slowly poured into the mixing drum and mixed thoroughly to produce a homogeneous fresh concrete.

Table 7. Mix proportions of the concretes.

Group	W/B	W (kg/m³)	C (kg/m³)	LWA (kg/m³)	FA (kg/m³)	SF (kg/m³)	PP (kg/m³)	SP (kg/m³)
Control group	0.45	220	489	345	734	58.5	1.17	0.978
Experimental group	0.45	220	489	345	734	58.5	1.17	0.978

Notes: W/B: water–binder ratio; W: water; C: cement; LWA: lightweight aggregate; FA: fine aggregate; SF: steel fiber; PP: polypropylene fiber; SP: superplasticizer.

2.5. Casting and Curing of Specimens

Concrete specimens were cast according to the relevant ASTM standards. The compression test used a cylindrical specimen with a diameter of 100 mm and a height of 200 mm. The pull-out test used a cubic specimen with a side length of 150 mm. A #6 steel bar with a diameter of 19.1 mm was embedded in the central axis of the pull-out specimen, and its embedded length (l_e) was three times the diameter of the steel bar (d_b), as shown in Figure 9. In addition, three transverse stirrups were configured to prevent the splitting failure of the specimen when the longitudinal steel bar was tensile. When casting the pull-out specimens, the non-bonded regions of the steel bar were wrapped with PVC sleeves. To prevent the steel bar of the specimen from being corroded during the curing process, water-based sealant was used to fill the gap between the PVC sleeves and the steel bar. After the mixing of each group of concrete was completed, the slump was measured immediately. Then, nine cylindrical specimens and nine pull-out specimens were cast for each set of concrete mixtures. The specimens were removed from the mold after twenty-four hours. The specimens from the control group and experimental group I were placed in a saturated lime water tank in a curing room. On the 14th day, the specimens were taken out and placed in a 40 °C incubator to cure until the test age, as shown in Figure 10a. The curing method of experimental group II specimens involved air curing in a 40 °C incubator for two days. Then, they were cured in a 40 °C curing solution (1 molar concentration of urea and 0.5 molar concentration of calcium acetate) for two days, as shown in Figure 10b. One curing cycle was four days.

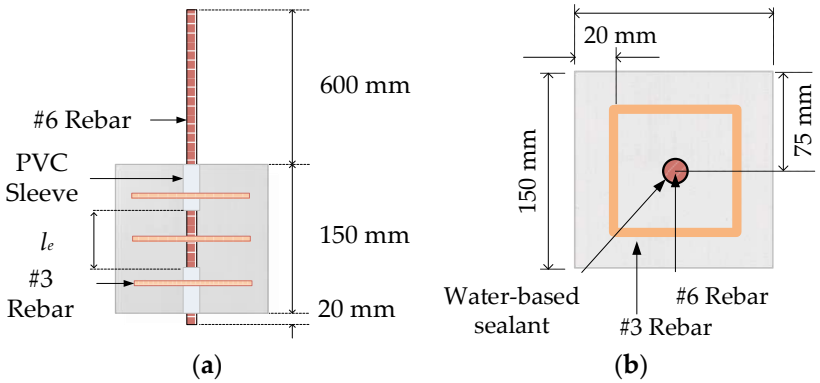

Figure 9. Dimensions and cross-sections of the pull-out specimens: (a) side view and (b) top view.

Preprints (www.preprints.org) | NOT PEER-REVIEWED | Posted: 20 November 2023 doi:10.20944/preprints202311.1233.v1

(a) (b)

Figure 10. Curing condition of the specimens (a) in an incubator and (b) in a curing solution tank.

2.6. Test Methods and Data Analysis

The testing methods for the various properties of concrete in this study were based on the ASTM specifications listed in Table 8. The compression test and elastic modulus test were conducted according to ASTM C39 and ASTM C469, respectively. The compressive strength and static elastic modulus values are the average values of three specimens. The pull-out test was performed in accordance with the specifications of ASTM C234. A 200 kN MTS servo valve-controlled machine equipped with a special test frame was used to apply a load to the specimen, as shown in Figure 11. In the pull-out specimen, one end of the steel bar is the load end, and the other end is the free end. Through the installation of three linear variable differential transformers (LVDT), the relative bond–slip between the steel bars and concrete at the load end and free end was measured. The transmission lines of the load and LVDT were connected to the data acquisition device, and the test was carried out after zeroing. The load was applied at a constant displacement rate of 0.01 mm/s during the pull-out test until the specimen failed. In addition to monitoring the test process on the computer screen, all load and displacement data were collected using a data logger and stored on a floppy disk.

Table 8. Test methods for concrete properties.

Item	Experiment Method
Slump	ASTM C143 [52]
Unit weight and air content	ASTM C138 [53]
Compressive strength	ASTM C39 [54]
Static modulus of elasticity	ASTM C469 [55]
Bond strength	ASTM C234 [56]

Figure 11. Setup of the pull-out test.

Through the pull-out test, the corresponding slip of the steel bars of the specimen under different loads was measured. As a result, the complete bond stress–slip relationship curve of the specimen

Preprints (www.preprints.org) | NOT PEER-REVIEWED | Posted: 20 November 2023 doi:10.20944/preprints202311.1233.v1

from loading to failure was obtained. In addition, the bond stress under different loads was obtained from the internal force balance of the specimen shown in Figure 12 [4]:

$$\tau = \frac{P}{\pi d_b l_e} \quad (5)$$

where τ is the bond stress; P is the applied load; d_b is the rebar diameter; and l_e is the embedded length. The relative slip between the steel bars and concrete corresponding to the bond stress can be divided into loading end slip (s_l) and free end slip (s_f). The free end slip referred to the relative displacement between the LVDT installed on the non-loaded side of the specimen and the steel bar at the free end. The slip at the loading end was the average value of the LVDT of the horizontal frame erected on the loading side of the specimen. The relative slip between the steel bars and concrete in the case of local bond can be regarded as rigid motion. Therefore, the average value of s_l and s_f was regarded as the slip corresponding to the bond stress, as shown in the following equation:

$$s = \frac{s_l + s_f}{2} \quad (6)$$

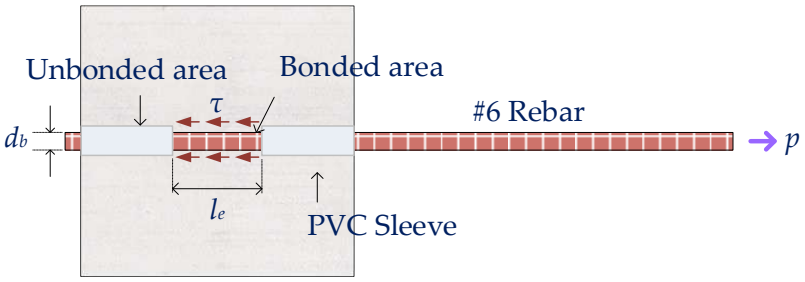

Figure 12. Schematic diagram of local bond stress between the rebar and concrete.

According to the different statuses of the specimen, the tests of the two groups of LWAC were divided into four types, as shown in Table 9. After the compression test was completed, samples were taken from two different parts of the two groups of cylindrical specimens (two centimeters away from the surface and the center). The purpose is to use FESEM and EDS to observe and analyze the microstructure of each group of concrete specimens after self-repair. The samples were cleaned, dried, and gold-plated before FESEM and EDS analysis. In addition, X-ray diffraction analysis was also used to conduct qualitative and semi-quantitative analyses of the element types and contents of each group of concrete samples.

Table 9. Test items and test sequences.

Test Item	Test Sequence
Compression test after 28 days of curing	Curing→loading
Secondary compression test after self-healing of compressive failure specimen	Curing→loading→self-healing→reloading
Pull-out test after 28 days of curing	Curing→loading
Secondary pull-out test after self-healing of pull-out failure specimen	Curing→loading→self-healing→reloading

3. Experimental Results and Discussions

3.1. Results of the Fresh Properties Test

Table 10 lists the slump and unit weight of the two groups of LWAC. As can be seen from Table 10, the slumps of the two groups of LWAC were both 13 cm, and both had good workability. In

 doi:10.20944/preprints202311.1233.v1

addition, the unit weight of both groups of LWAC was 1849 kg/m^3, which was only 80.4% of that of ordinary NWC.

Table 10. Fresh properties of the LWAC.

Group	Slump (cm)	Unit Weight (kg/m^3)
Control group	13	1849
Experimental group	13	1849

3.2. Results of the Compression Test

3.2.1. Compressive Strength and Elastic Modulus of First Compression Test

Table 11 lists the 28-day compressive strength test results of the two groups of LWAC. The values were very close to the required compressive strength (i.e., 45 MPa). As can be seen from Table 11, the 28-day compressive strength of the two groups of LWAC was the same, ranging from 44.59 to 45.88 MPa. Among them, experimental group II had the highest value of 45.88 MPa, followed by experimental group I at 44.81 MPa, and the control group had the lowest value at 44.59 MPa. The structural efficiency (strength/density) of the two groups of LWAC was 24.3 MPa/(t/m^3), which was within the range of most LWACs, that is, 10–40 MPa/(t/m^3) [57]. In addition, the 28-day elastic modulus of the two groups of LWAC was roughly similar, ranging from 18.75 to 19.26 GPa. Among them, experimental group II had the highest value of 19.26 GPa, followed by experimental group I at 19.09 GPa, and the control group had the lowest value of 18.75 GPa. The elastic modulus of typical expanded clay LWA was in the range of 10–20 GPa [58,59]. Therefore, the results are consistent with the literature.

Table 11. Test results of compressive strength and elastic modulus of the LWACs.

Group	Compressive Strength (MPa)	Elastic Modulus (GPa)
Control group	44.59	18.75
Experimental group I	44.81	19.09
Experimental group II	45.88	19.26

3.2.2. Compressive Strength of Secondary Compression Test

The cylindrical specimens of the two groups of LWAC after the compression test were cured. The results of the secondary compressive strength test after 28 days of self-healing are shown in Table 12. As can be seen from Table 12, after 28 days of self-healing, the compressive strengths of the control group, experimental group I, and experimental group II were 13.83, 14.37, and 15.61 MPa, respectively. In addition, the residual compressive strength after self-healing was divided by the original 28-day compressive strength to calculate the relative compressive strength ratio, as shown in Table 12. As can be clearly seen from Table 12, the relative compressive strength ratios of the control group, experimental group I, and experimental group II after 28 days of self-healing were 0.31, 0.32, and 0.34, respectively. Compared with the control group, the relative compressive strength ratio of experimental group I increased by 3.2%, and the relative compressive strength ratio of experimental group II increased by 9.7%. This shows that the curing method of experimental group II had a better self-healing effect.

Table 12. Results of secondary compressive test of cylindrical specimens after self-healing.

Group	Compressive Strength (MPa)	Residual Compressive Strength after Self-Healing (MPa)	Relative Compressive Strength Ratio after Self-Healing

 doi:10.20944/preprints202311.1233.v1

Control group	44.59	13.83	0.31
Experimental group I	44.81	14.37	0.32
Experimental group II	45.88	15.61	0.34

3.3. Results of the Pull-Out Test

3.3.1. Bond Strength of First Pull-Out Test

The failure modes of the pull-out specimens in both groups of LWAC were shear pull-out failures. This test was characterized by the center steel bar being pulled out of the concrete and a small number of cracks appearing in the surrounding concrete. Based on the data captured during the pull-out test, the maximum bond stress (i.e., bond strength) of the pull-out specimen could be analyzed. The first pull-out test results for each group of specimens are shown in Table 13. As can be seen from Table 13, the 28-day average bond strength of both groups of LWACs was close to 28 MPa. This result exceeds the recommended value of Mo et al. [21] ($3.5\sqrt{f_c'}$) and the recommended value of the CEB-FIP standard ($2.5\sqrt{f_c'}$) [24]. This is because LWA has a stronger aggregate interlocking effect and the content of binder material in LWAC is higher, which improves the quality of the cement slurry and, thus, improves the mechanical interlocking performance [21,23]. This result is consistent with the results of Kevinly et al. [60].

Table 13. Results of first pull-out test.

Group	Bond Strength (MPa)	Failure Mode
Control group	27.99	Pull-out
Experimental group I	28.38	Pull-out
Experimental group II	28.02	Pull-out

3.3.2. Bond Strength of Secondary Pull-Out Test

The two groups of LWAC specimens after the pull-out test were cured. The results of the secondary pull-out test after 28 days of self-healing are shown in Table 14. As can be seen from Table 14, after 28 days of self-healing, the residual bond strengths of the control group, experimental group I, and experimental group II were 18.84, 20.82, and 22.25 MPa, respectively. In addition, the residual bond strength after self-healing was divided by the original bond strength to calculate the relative bond strength ratio, as shown in Table 14. As can be clearly seen from Table 14, the relative bond strength ratios of the control group, experimental group I, and experimental group II after 28 days of self-healing were 0.67, 0.73, and 0.79, respectively. Compared with the specimens in the control group, the relative bond strength ratios of experimental groups I and II increased by 9% and 17.9%, respectively. This shows that after 28 days of self-healing, experimental group II had the highest relative bond strength ratio. Once again, this showed that the curing method used in experimental group II had a better self-healing effect.

Table 14. Results of secondary pull-out test.

Group	Bond Strength (MPa)	Residual Bond Strength (MPa)	Relative Bond Strength Ratio
Control group	27.99	18.84	0.67
Experimental group I	28.38	20.82	0.73
Experimental group II	28.02	22.25	0.79

3.4. Local Bond Stress–Slip Relationship of Steel Bars in LWAC

3.4.1. Bond Stress–Slip Relationship in the First Pull-Out Test of Steel Bars in LWAC

 doi:10.20944/preprints202311.1233.v1

Due to the lower strength of LWA, the bond behavior between LWAC and steel bars is different from that between NWC and steel bars [12]. However, there is a lack of a unified understanding of this difference. Therefore, the current research on the bond stress–slip relationship between LWAC and steel bars is mostly determined through experiments [4,21,61]. An analysis of the literature data shows [62,63] that the ratio of concrete protective layer to steel bar diameter (*C*/*D*) in the range of 2.5–3.0 can ensure that the failure mode is pull-out failure. The concrete protective layer of the pull-out specimen in this study was relatively thick (6.5 cm), and its *C*/*D* ratio was 3.4. Furthermore, the specimen had transverse stirrups. As a result, the longitudinal steel bar of the specimen was subject to greater confinement, and the concrete between the transverse bars was sheared due to punching, causing the steel bars to be pulled out directly from the concrete. In other words, all specimens showed a pull-out failure mode, as shown in Figure 13.

(**a**) (**b**) (**c**)

Figure 13. Damage conditions of the LWAC specimen in the first pull-out test: (**a**) control group, (**b**) experimental group I, and (**c**) experimental group II.

In the first pull-out test, the test was stopped when the steel bar slipped 5 mm to avoid further damage. In the subsequent analysis, the first pull-out test of each group of specimens only focused on the slip of the steel bars in the range of 0–5 mm. The local bond stress–slip relationship curves of the two groups of LWAC specimens are shown in Figure 14. As can be seen from Figure 14, during the test process, the slip relationship curves of each group of specimens experienced linear ascending, non-linear ascending, and descending stages. In the linear ascending stage, the specimen was not cracked and was in an elastic state; in the non-linear ascending stage, the cracks in the specimen gradually expanded; in the descending stage, the specimen showed obvious cracks. It is worth noting that the ascending branch of the bond stress–slip curve of the two groups of LWAC had a more linear relationship. This is because LWAC's cementitious matrix provided better chemical adhesion and greater tensile strength. This is consistent with the literature [4]. In addition, the ultimate bond stress of the first pull-out test of the experimental group was slightly higher than that of the control group, but the corresponding slip amount s_1 was smaller, with a value of about 1-3 mm. The comparison between the local bond stress–slip relationship curve obtained from the pull-out test and the prediction model is shown in Figure 15. As can be seen from Figure 15, the ultimate bond stress of the two groups of LWAC was significantly higher than the predicted values of the models of MC 2010 [24] and Harajli et al. [32]. This means that the models of MC 2010 [24] and Harajli et al. [32] are too conservative for estimating the ultimate bond stress of LWAC.

Preprints (www.preprints.org) | NOT PEER-REVIEWED | Posted: 20 November 2023 doi:10.20944/preprints202311.1233.v1

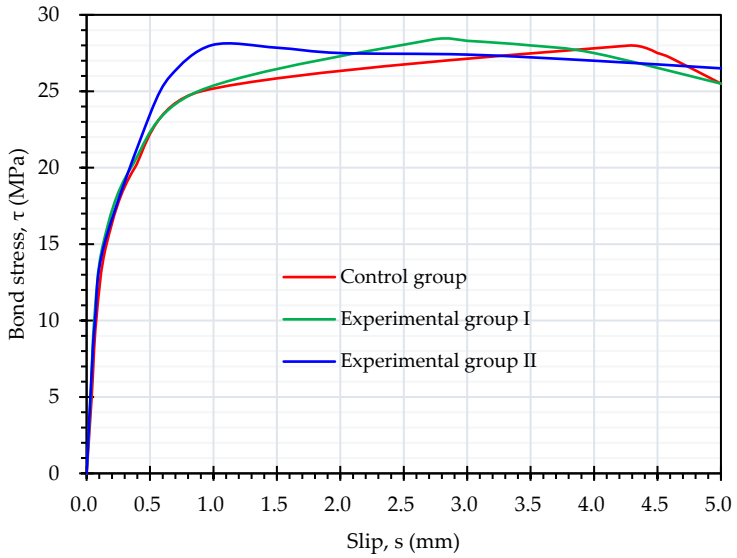

Figure 14. Local bond stress–slip relationship for the first pull-out test.

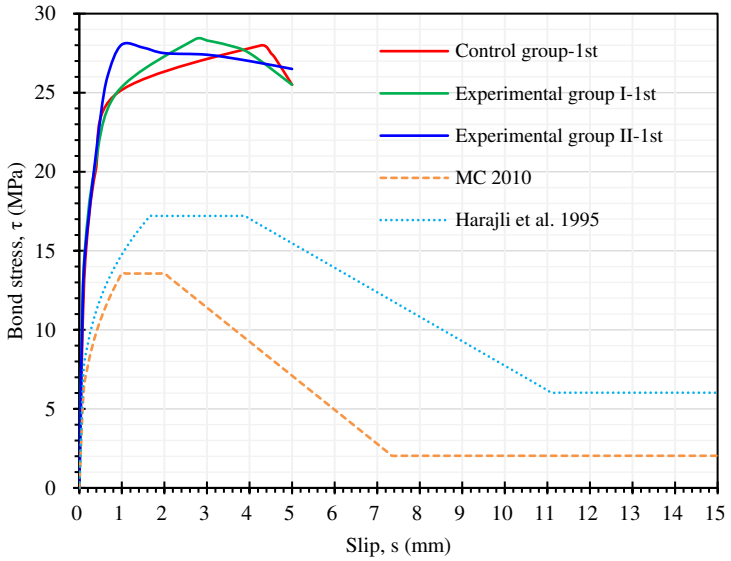

Figure 15. Comparison of first local bond stress–slip curve with the prediction models.

3.4.2. Bond Stress–Slip Relationship in the Secondary Pull-Out Test of Steel Bars in LWAC

According to the planned curing method, the pull-out specimens that had undergone shear pull-out failure were cured. After the two groups of LWAC specimens had self-cured for 28 days, the secondary pull-out test was conducted. In the secondary pull-out test of the specimen, the test did not stop even if the slip of the steel bar reached 5 mm. Instead, the test continued until the specimen failed completely, as shown in Figure 16.

(**a**) (**b**) (**c**)

 doi:10.20944/preprints202311.1233.v1

Figure 16. Damage conditions of the LWAC specimens in the secondary pull-out test: (**a**) control group, (**b**) experimental group I, and (**c**) experimental group II.

Figure 17 shows that the two groups of LWAC specimens still exhibited linear ascending and non-linear ascending stages after self-healing. In addition, there was a plateau section where the bond stress decreased slowly, but the slip continued to increase. Subsequently, a more obvious attenuation occurred. In the residual stage, LWAC generated bond stress through friction. In other words, the bond stress–slip relationship in the secondary pull-out test of the two groups of LWAC specimens was divided into four stages: linear ascending, non-linear ascending, descending, and residual stages, as shown in CEB-FIP 2000 [24]. Comparing the bond stress–slip curves in the first and secondary pull-out tests of the two groups of specimens shows that the ultimate bond stress in the secondary pull-out test was significantly reduced. Nonetheless, a comparison of the local bond stress–slip relationship curve obtained from the secondary pull-out test with the prediction model is shown in Figure 18. As can be seen from Figure 18, the ultimate bond stress of the two groups of LWAC was still higher than the predicted value of the models of MC 2010 [24] and Harajli et al. [32]. It is worth noting that the ultimate bond stress of the experimental group specimens in the secondary pull-out test was significantly higher than that of the control group. In particular, the ultimate bond stress of the specimens in experimental group II was 17.9% higher than that of the control group specimens. This is due to the different maintenance environments for each group of specimens.

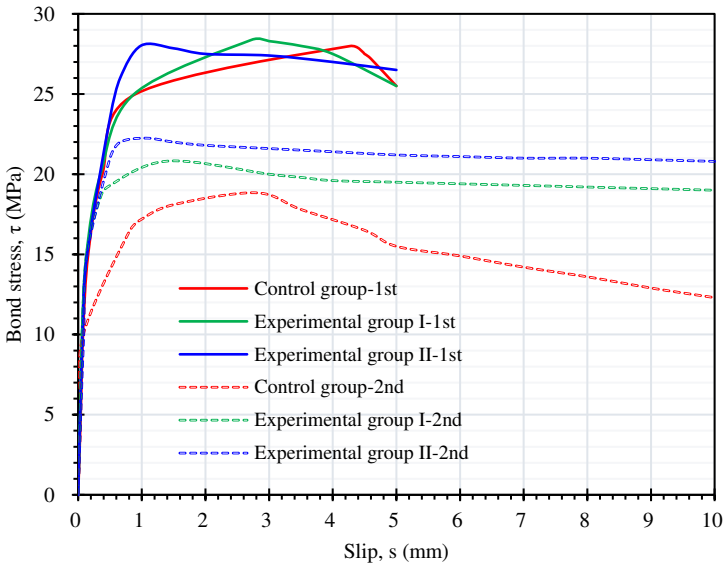

Figure 17. Comparison of local bond stress–slip relationships between the first and second pull-out tests.

Preprints (www.preprints.org) | NOT PEER-REVIEWED | Posted: 20 November 2023 doi:10.20944/preprints202311.1233.v1

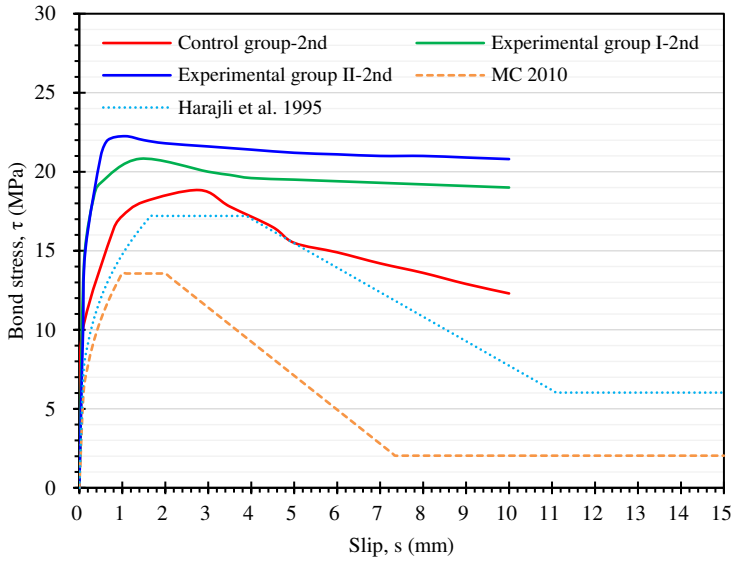

Figure 18. Comparison of secondary local bond stress–slip curve with the prediction models.

3.5. Result of the Concrete Crack Healing Observation

For the cylindrical specimen, the self-healing of the cracks formed in the compression test was observed. The size and location of these cracks were difficult to control. Therefore, only cracks on the surface were observed, as shown in Figure 19. For the specimens in the control group and experimental group I, as the curing age increased, the self-healing of the cracks was not obvious, as shown in Figure 19a,b. In contrast, starting on the seventh day, calcium carbonate crystals began to crystallize in the cracks on the surface of the experimental group II specimen, as shown in Figure 19c. Moreover, as the curing period increased, the crystals tended to become denser and more extensive. This result showed that the self-healing effect of cracks in each group of specimens was closely related to the curing environment.

Group	Self-Healing Age		
	0 Days	7 Days	14 Days
Control group			
Experimental group I			

Preprints (www.preprints.org) | NOT PEER-REVIEWED | Posted: 20 November 2023 doi:10.20944/preprints202311.1233.v1

Figure 19. Self-healing of cracks in cylindrical specimens.

3.6. Results of FESEM Images, EDS Analysis, and XRD Analysis

3.6.1. Results of FESEM Images

After the first compression test, samples were taken at 2 cm from the surface of the cylindrical specimen and at the center. The endospore of *S. pasteurii* bacteria was observed near the surface and in the center of the specimen, as shown in Figure 20. In addition, calcium carbonate blocks appeared around the strains.

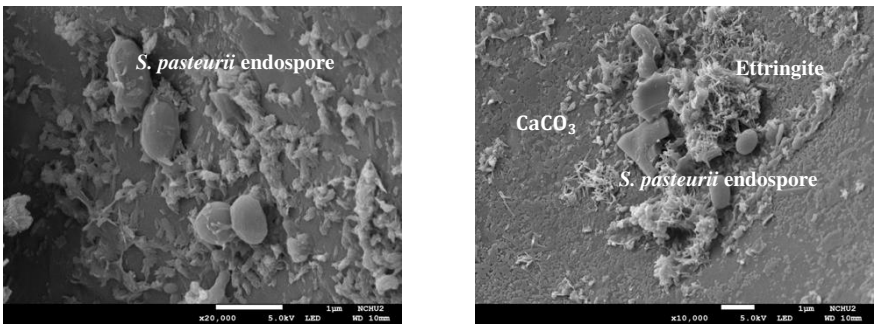

(**a**) (**b**)

Figure 20. FESEM images of the experimental group sample with a self-healing age of 0 days (**a**) taken from the surface block and (**b**) taken from the center block.

Moreover, after 28 days of self-healing of the cylindrical specimen, samples were also taken at 2 cm from the surface of the cylindrical specimen and at the center. Figure 21 shows the FESEM images of the two groups of LWAC samples after 28 days of self-healing. The figure reveals information about the pore structure, cracks, and mineral phases in the two groups of concrete samples. Among them, the slender hexagonal needles were ettringite (AFt), the hexagonal plates were calcium hydroxide (CH), the network floc was calcium silicate hydrate (C-S-H) colloid, and the black parts were pores in the matrix. In addition, lightweight aggregate and ITZ could also be seen. As can be seen from Figure 21, the ITZ of the control group and experimental group I had the same density. Many calcium carbonate crystal particles with parallel polygonal cubic structures were found on the surface of the block in experimental group II. In other words, there were obvious white calcite clusters in the experimental group II samples. This result confirmed that the samples of experimental group II had microbially induced calcium carbonate precipitation (MICP) [64]. During the MICP process, the metabolic activity of microorganisms increased the local saturation state of bacterial cells. This promoted the precipitation of $CaCO_3$ [65]. Therefore, experimental group II could achieve better repair and healing effects, thus improving its performance.

Preprints (www.preprints.org) | NOT PEER-REVIEWED | Posted: 20 November 2023 doi:10.20944/preprints202311.1233.v1

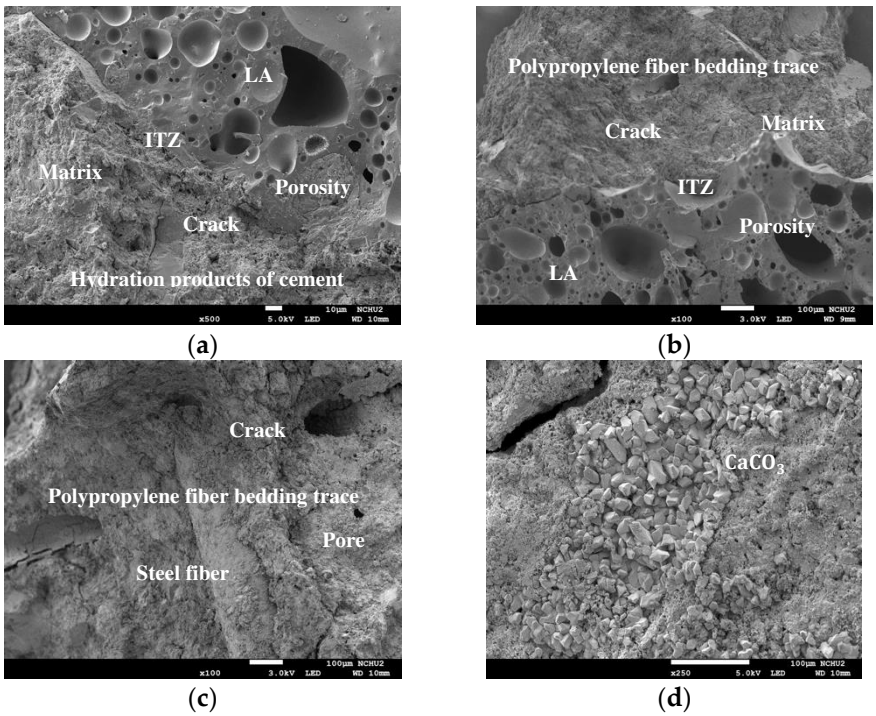

Figure 21. FESEM images of the surface blocks of each group of samples with a self-healing age of 28 days: (**a**) control group, (**b**) experimental group I, (**c**) experimental group II (100 × magnification), and (**d**) experimental group II (250 × magnification).

3.6.2. Results of EDS Analysis

The EDS test was performed at the interface between the LWA and the matrix of the FESEM-observed sample that had been left to self-heal for 28 days. It mainly analyzed the weight percentages of various chemical elements in the sample. The EDS spectra of each group of samples are shown in Figure 22. The y-axis in the figure describes the number of X-rays, and the x-axis is the energy of the X-rays. In addition, the position of the peak is the identification of the element, and the peak height helps to quantify the content of each element in the sample. From the EDS analysis, the elements contained in each group of samples were C ($CaCO_3$, calcium carbonate), O (SiO_2, silicon dioxide), Mg (MgO, magnesium oxide), Al (Al_2O_3, aluminum oxide), Si (SiO_2, silicon dioxide), K (MAD-10 Feldspar, feldspar), Ca (Wollastonite, calcium silicate), Fe (iron), S (FeS_2, iron disulfide), Na (Albite, albite), and other elements. It is worth noting that in the precipitation-filled crack region of the experimental group II sample, Ca, C, and O bonded to form $CaCO_3$. This result confirmed that microbial mineralization occurred in the experimental group II samples [64]. Therefore, experimental group II achieved better performance compared to the control group.

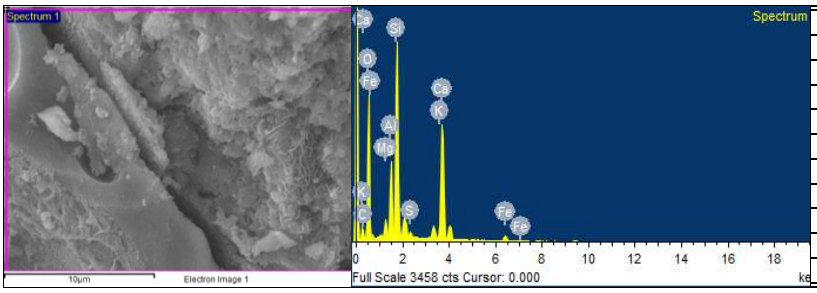

Element	Weight%	Atomic%
C K	6.87	11.50
O K	49.33	62.01
Mg K	1.14	0.94
Al K	5.13	3.83
Si K	14.76	10.57
S K	0.60	0.38
K K	1.77	0.91
Ca K	17.83	8.95
Fe K	2.56	0.92
Totals	100.00	100.00

(**a**)

Preprints (www.preprints.org) | NOT PEER-REVIEWED | Posted: 20 November 2023 doi:10.20944/preprints202311.1233.v1

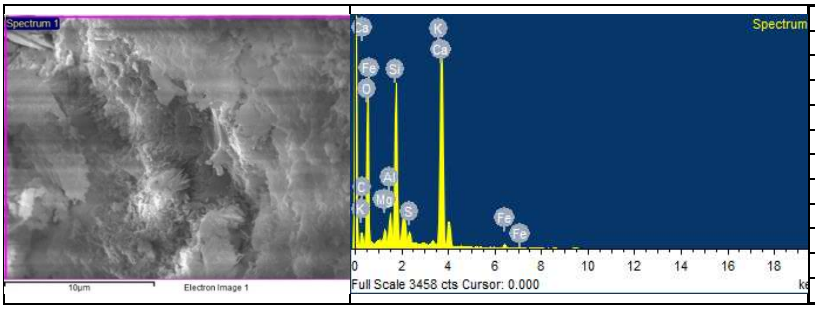

Element	Weight%	Atomic%
C K	4.55	7.73
O K	53.45	68.11
Mg K	0.86	0.72
Al K	1.50	1.13
Si K	10.17	7.39
S K	1.09	0.69
K K	0.43	0.22
Ca K	26.49	13.48
Fe K	1.47	0.54
C K	4.55	7.73
Totals	100.00	100.00

(**b**)

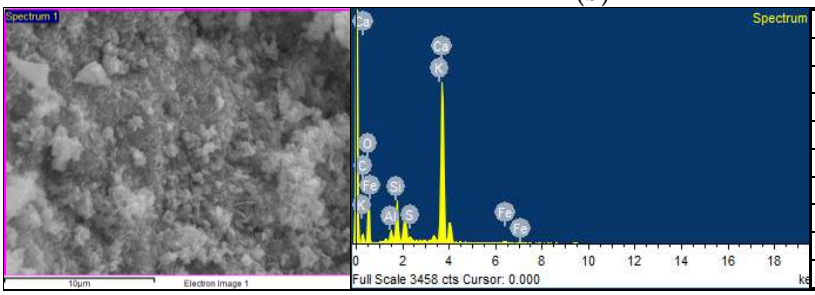

Element	Weight%	Atomic%
C K	6.97	12.84
O K	41.38	57.25
Al K	1.23	1.01
Si K	5.10	4.02
S K	0.80	0.55
K K	1.14	0.65
Ca K	41.61	22.98
Fe K	1.77	0.70
Totals	100.00	100.00

(**c**)

Figure 22. EDS analysis results of each group of samples with a self-healing period of 28 days: (**a**) control group, (**b**) experimental group I, and (**c**) experimental group II.

3.6.3. Results of XRD Analysis

X-ray diffraction (XRD) analysis can provide information about the phases and compounds present in a sample. In view of this, XRD analysis was performed on the LWAC samples to determine their mineral composition. In comparison with the material crystal standard card of the inorganic crystal structure database (ICSD) and the crystallographic information file (CIF) of the material, the XRD analysis results of each group of samples were obtained, as shown in Figure 23. As can be seen from Figure 23, the main reflection angles (2-theta) of the calcium carbonate crystal (reference code: 01-086-2343) were 30.6°, 36.5°, and 43.1°. In addition, the X-ray reflection energy intensity of the experimental group at all angles was higher than that of the control group. Quartz crystal (reference code: 01-089-3755) had main reflection angles (2-theta) of 20.8° and 26.5°. The main reflection angles of calcium hydroxide crystals (reference code: 01-089-1263) were (2-theta) 18.0° and 34.1°. The X-ray reflected energy intensity at all angles in the experimental group was lower than that in the control group. This indicated that the addition of the *S. pasteurii* strain could effectively reduce the formation of calcium hydroxide (CH) crystals. In addition, it could be converted into cubic crystals and agglomerated materials composed of other structures. Due to the poor composition of the CH crystal structure, its contribution to strength is low. This can verify that experimental group II in the secondary compression test and the secondary pull-out test of this study did have higher strength.

Preprints (www.preprints.org) | NOT PEER-REVIEWED | Posted: 20 November 2023 doi:10.20944/preprints202311.1233.v1

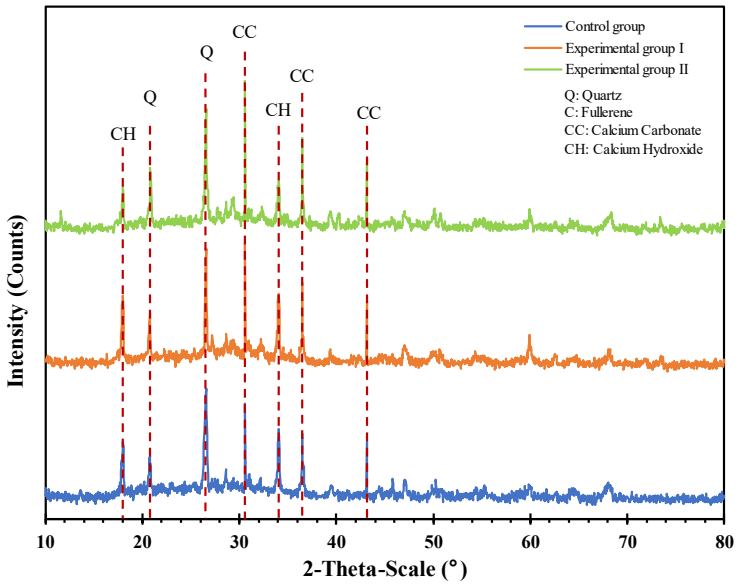

Figure 23. XRD analysis of each group of samples with a self-healing period of 28 days.

4. Conclusions

The self-healing of concrete cracks can improve the concrete's durability and sustainability, thereby extending the service life of concrete structures. This study applied biomineralization to repair damaged fiber-reinforced LWAC. After the damaged specimen healed itself for 28 days, the secondary compression test and the secondary pull-out test were conducted. The relative compressive strength ratios of the control group, experimental group I, and experimental group II were 0.31, 0.32, and 0.34, respectively. Compared with the control group, the relative compressive strength ratio of experimental group I increased by 3.2%, and the relative compressive strength ratio of experimental group II increased by 9.7%. However, the relative bond strength ratios of the control group, experimental group I, and experimental group II were 0.67, 0.73, and 0.79, respectively. Compared with the specimens in the control group, the relative bond strength ratios of the experimental group I and experimental group II specimens increased by 9% and 17.9%, respectively. In particular, the ultimate bond stress ratio of the experimental group II specimens was significantly higher than that of the control group. Moreover, the EDS and XRD analysis results confirmed that the precipitate formed at the crack was calcium carbonate, which improved the compressive strength and bond strength after self-healing. This indicates that the biomineralization maintenance method used in experimental group II is more effective.

Author Contributions: Conceptualization, H.-J.C. and C.-W.T.; methodology, H.-J.C. and C.-W.T.; software, C.-W.T. and H.-W.C.; validation, H.-J.C. and T.-K.C.; formal analysis, C.-W.T.; investigation, H.-J.C. and T.-K.C.; resources, C.-W.T.; data curation, H.-J.C., H.-W.C., and T.-K.C.; writing—original draft preparation, H.-J.C. and C.-W.T.; writing—review and editing, C.-W.T.; visualization, H.-W.C.; supervision, C.-W.T. and H.-W.C.; project administration, C.-W.T.; funding acquisition, C.-W.T. All authors have read and agreed to the published version of the manuscript.

Funding: This research was funded by the Ministry of Science and Technology of Taiwan, grant number MOST 110-2221-E-230-001-MY3.

Institutional Review Board Statement: Not applicable.

Informed Consent Statement: Not applicable.

Data Availability Statement: The data presented in this study are available upon request from the corresponding author.

Acknowledgments: The authors are grateful to the Department of Civil Engineering of National Chung-Hsing University for providing the experimental equipment and technical support. In addition, the authors thank Dr. Yi-Hao Guo from the Chunmin Construction Company for providing bacterial solutions and technical support.

Conflicts of Interest: The authors declare no conflict of interest.

References

1. Somayaji, S. Civil engineering materials, 3rd ed. New Jersey: Prentice Hall, 2001.
2. ACI Committee 213. ACI 213R-03; Guide for Structural Lightweight Aggregate Concrete. American Concrete Institute: Farmington Hills, MI, USA, 2003.
3. Chandra, S. and Berntsson, L. Lightweight Aggregate Concrete, Noyes Publications, New York, USA, 2002
4. Tang, C.-W. Local bond stress-slip behavior of reinforcing bars embedded in lightweight aggregate concrete. *Computers & Concrete* **2015**, *16(3)*, 449–466. https://doi.org/10.12989/cac.2015.16.3.449
5. Tang, C.-W. Uniaxial bond stress-slip behavior of reinforcing bars embedded in lightweight aggregate concrete. *Structural Engineering and Mechanics* ***2017***, *62(5)*, 651–661. https://doi.org/10.12989/sem.2017.62.5.651
6. Gao, J.; Suqa, W.; Morino, K. Mechanical properties of steel fiber-reinforced, high-strength, lightweight concrete. *Cem Concr Compos.* **1997**, *19*, 307–313. https://doi.org/10.1016/S0958-9465(97)00023-1
7. Hassanpour, M.; Shafigh, P.; Mahmud, H.B. Lightweight aggregate concrete fiber reinforcement—A review. *Constr. Build. Mater.* **2012**, *37*, 452–461. https://doi.org/10.1016/j.conbuildmat.2012.07.071
8. Ding, Y.; Kusterle, W. Compressive stress–strain relationship of steel fibre reinforced concrete at early age. *Cem Concr Res* **2000**, *30*, 1573–1579. https://doi.org/10.1016/S0008-8846(00)00348-3
9. Li, V.C. Large volume high performance applications of fibers in civil engineering. *J Appl Polym Sci* ***2002***, *83(3)*, 660–686. https://doi.org/10.1002/app.2263
10. Metha, P.K.; Monteiro, P.J.M. Concrete: Microstructure, Properties and Materials, 3rd Ed.; McGraw-Hill: New York, NY, USA, 2006.
11. Zhao, M.; Zhao, M.; Chen, M.; Li, J.; Law, D. An experimental study on strength and toughness of steel fiber reinforced expanded-shale lightweight concrete. *Constr. Build. Mater.* **2018**, *183*, 493–501. https://doi.org/10.1016/j.conbuildmat.2018.06.178
12. Wang, B.; Zhu, E.; Zhang, Z.; Zhu, C. Bond-slip behaviour of lightweight aggregate concrete based on virtual crack model with exponential softening characteristics. *Constr. Build. Mater.* **2022**, *345*, 128349. https://doi.org/10.1016/j.conbuildmat.2022.128349
13. Huang, L.; Chi, Y.; Xu, L.; Chen, P.; Zhang, A. Local bond performance of rebar embedded in steel-polypropylene hybrid fiber reinforced concrete under monotonic and cyclic loading. *Constr. Build. Mater.* **2016**, *103*, 77–92. https://doi.org/10.1016/j.conbuildmat.2015.11.040
14. Wu, Z.M.; Shi, C.J.; Khayat, K.H. Multi-scale investigation of microstructure, fiber pullout behavior, and mechanical properties of ultra-high performance concrete with nano-$CaCO_3$ particles. *Cem Concr Compos* **2018**, *86*, 255–65. https://doi.org/10.1016/j.cemconcomp.2017.11.014
15. Campione, G.; Cucchiara, C.; La Mendola, L.; Papia, M. Steel–concrete bond in lightweight fiber reinforced concrete under monotonic and cyclic actions. *Eng. Struct.* **2005**, *27(6)*, 881–890. https://doi.org/10.1016/j.engstruct.2005.01.010
16. ACI Committee. 408. Bond and development of straight reinforcing bars in tension (ACI 408R–03). Farmington Hills, MI: American Concrete Institute; 2003.
17. ACI Committee 318-19, Building Code Requirements for Structural Concrete and Commentary, American Concrete Institute, Farmington Hills (2019).
18. Lutz, L.A.; Gergely, P. Mechanics of Bond and Slip of Deformed Reinforcement. *ACI J.* **1967**, *64*, 711–721.
19. Bond stress-slip relationship of oil palm shell lightweight concrete. *Eng Struct* **2016**, *127*, 319–30. https://doi.org/10.1016/j.engstruct.2016.08.064
20. Hossain, K.M.A. Bond characteristics of plain and deformed bars in lightweight pumice concrete. *Constr. Build. Mater.* **2008**, *22(7)*, 1491–2149. https://doi.org/10.1016/j.conbuildmat.2007.03.025
21. Mo, K.H.; Alengaram, U.J.; Visintin, P.; Goh, S.H.; Jumaat, M.Z. Influence of lightweight aggregate on the bond properties of concrete with various strength grades. *Constr. Build. Mater.* **2015**, *84*, 377–86. https://doi.org/10.1016/j.conbuildmat.2015.03.040
22. Liu, Y.; Liu, X.; Wu, T.; Luo, X.; Feng, W. Bond-slip behavior between corroded rebar and lightweight aggregate concrete. *Constr. Build. Mater.* **2023**, *367*, 130268. https://doi.org/10.1016/j.conbuildmat.2022.130268
23. Yang, X.; Wu, T.; Liu, X.; Liu, Y. Bond-slip relationship of rebar in lightweight aggregate concrete. *Structures* **2022**, *45*, 2198–2209. https://doi.org/10.1016/j.istruc.2022.10.010
24. CEB-FIP. Fib Model Code for Concrete Structures 2010; Comité Euro international du Béton/Federation Internationale de la Precontrainte: Lausanne, Switzerland, 2013.
25. Shima, H.; Chou, L.L.; Okamura, H. Micro and macro models for bond in reinforced concrete. *J. Fac. Eng.* **1987**, *39*, 133–194.
26. Kankam, C.K. Relationship of bond stress, steel stress, and slip in reinforced concrete. *J. Struct. Eng.* **1997**, *123(1)*, 79–85. https://doi.org/(ASCE)0733-9445(1997)123:1(79)

27. Eligehausen, R.; Popov, E.P.; Bertero, V.V. Local bond stress-slip relationships of deformed bars under generalized excitations. University of California, Berkeley, USA, 1983.
28. Filippou, F.C.; Popov, E.P.; Bertero, V.V. Modeling of R/C joints under cyclic excitations. *J. Struct. Eng.* **1983**, *109*, 2666–2684. https://doi.org/10.1061/(ASCE)0733-9445(1983)109:11(2666)
29. Saeed, M.N. Internal measurement of bond stress slip relationship in reinforced concrete. *ACI J.* **1979**, *76*, 19.
30. Pauletta, M.; Rovere, N.; Randl, N.; Russo, G. Bond-Slip Behavior between Stainless Steel Rebars and Concrete. *Materials* **2020**, *13*, 979. https://doi.org/10.3390/ma13040979.
31. CEB (1992), *CEB-FIP Model. Code 90*, Thomas Telford, London, UK, 1992.
32. Harajli, M.H.; Hout, M.; Jalkh, W. Local bond stress-slip behaviour of reinforcing bars embedded in plain and fibre concrete. *ACI Mater. J.* **1995**, *92(4)*, 343-353. https://doi.org/10.14359/999
33. Harajli, M. H.; Hamad, B.; Karam, K. Bond-slip Response of Reinforcing Bars Embedded in Plain and Fiber Concrete. *J. Mater. Civil Eng.* **2002**, *14(6)*, 503–511. https://doi.org/10.1061/(ASCE)0899-1561(2002)14:6(503)
34. Harajli, M.H. Numerical bond analysis using experimentally derived local bond laws: A powerful method for evaluating the bond strength of steel bars. *J. Struct. Eng.* **2007**, *133(5)*. 695-705. https://doi.org/10.1061/(ASCE)0733-9445(2007)133:5(695)
35. Hermawan, H.; Wiktor, V.; Gruyaert, E.; Serna, P. Experimental investigation on the bond behaviour of steel reinforcement in self-healing concrete. *Constr. Build. Mater.* **2023**, *383*, 131378. https://doi.org/10.1016/j.conbuildmat.2023.131378
36. Sierra-Beltran, M.G.; Jonkers, H.M.; Schlangen, E. Characterization of sustainable bio-based mortar for concrete repair. *Constr. Build. Mater.* **2014**, 67, 344–352. https://doi.org/10.1016/j.conbuildmat.2014.01.012
37. Dry, C.M. Three designs for the internal release of sealants, adhesives, and waterproofing chemicals into concrete to reduce permeability. *Cem. Concr. Res.* **2000**, *30*, 1969–1977. https://doi.org/10.1016/S0008-8846(00)00415-4
38. Iheanyichukwu, C.G.; Umar, S.A.; Ekwueme, P.C. A Review on Self-Healing Concrete Using Bacteria. *Sustain. Struct. Mater. Int. J.* **2018**, *1*, 12–20. https://doi.org/10.26392/SSM.2018.01.01.012
39. Zhang, K.; Tang, C.S.; Jiang, N.J.; Pan, X.H.; Liu, B.; Wang, Y.J.; Shi, B. Microbial induced carbonate precipitation (MICP) technology: a review on the fundamentals and engineering applications. *Environ. Earth Sci.* **2023**, *82*, 229. https://doi.org/10.1007/s12665-023-10899-y
40. Stanaszek-Tomal, E. Bacterial Concrete as a Sustainable Building Material?. *Sustainability* **2020**, *12*, 696. https://doi:10.3390/su12020696
41. Xu, J.; Wang, X.; Zuo, J.; Liu, X. Self-healing of concrete cracks by ceramsite-loaded microorganisms. *Adv. Mater. Sci. Eng.* **2018**, 2018, 5153041. https://doi.org/10.1155/2018/5153041.
42. Feng, C.; Zong, X.; Cui, B.; Guo, H.; Zhang, W.; Zhu, J. Application of Carrier Materials in Self-Healing Cement-Based Materials Based on Microbial-Induced Mineralization. *Crystals* **2022**, *12*, 797. https://doi.org/10.3390/cryst12060797
43. Jonkers, H.M.; Thijssen, A.; Muyzer, G.; Copuroglu, O.; Schlangen, E. Application of bacteria as self-healing agent for the development of sustainable concrete. *Ecol. Eng.* **2010**, *36*, 230–235. https://doi.org/10.1016/j.ecoleng.2008.12.036
44. Chen, H.-J.; Chang, H.-L.; Tang, C.-W.; Yang, T.-Y. Application of biomineralization technology to self-healing of fiber-reinforced lightweight concrete after high temperatures. *Materials* **2022**, *15(21)*, 7796. https://doi.org/10.3390/ma15217796
45. Menon, R.R.; Luo, J.; Chen, X.; Zhou, H.; Liu, Z.; Zhou, G.; Zhang, N.; Jin, C. Screening of fungi for potential application of self-healing concrete. *Sci. Rep.* **2019**, *9*, 2075. https://doi.org/10.1038/s41598-019-39156-8.
46. Jiang, L.; Jia, G.; Wang, Y.; Li, Z. Optimization of Sporulation and Germination Conditions of Functional Bacteria for Concrete Crack-Healing and Evaluation of their Repair Capacity. *ACS Appl. Mater. Interfaces* **2020**, *12*, 10938–10948. https://doi.org/10.1021/acsami.9b21465.
47. Reeksting, B.J.; Hoffmann, T.D.; Tan, L.; Paine, K.; Gebhard, S. In-depth profiling of calcite precipitation by environmental bacteria reveals fundamental mechanistic differences with relevance to application. *Appl Environ. Microbiol* **2020**, *86*, e02739-19. https://doi.org/10.1128/AEM.02739-19.
48. Hermawan, H.; Minne, P.; Serna, P.; Gruyaert, E. Understanding the Impacts of Healing Agents on the Properties of Fresh and Hardened Self-Healing Concrete: A Review. *Processes* **2021**, *9*, 2206. https://doi.org/10.3390/pr9122206
49. Chen, H.-J.; Peng, C.-F.; Tang, C.-W.; Chen, Y.-T. Self-Healing Concrete by Biological Substrate. *Materials* **2019**, *12*, 4099. https://doi.org/10.3390/ma12244099
50. ASTM C494/C494M-17; Standard and Specification for Chemical Admixtures for Concrete. ASTM International: West Conshohocken, PA, USA, 2017.
51. ASTM A820/A820M-06; Standard Specification for Steel Fibers for Fiber-Reinforced Concrete. ASTM International: West Conshohocken, PA, USA, 2006.
52. ASTM C143/C143M-15a; Standard Test Method for Slump of Hydraulic-Cement Concrete. ASTM International: West Conshohocken, PA, USA, 2015.

53. ASTM C138/C138M-17a; Standard Test Method for Density (Unit Weight), Yield, and Air Content (Gravimetric) of Concrete. ASTM International: West Conshohocken, PA, USA, 2017.
54. ASTM C39/C39M-18; Standard Test Method for Compressive Strength of Cylindrical Concrete Specimens. ASTM International: West Conshohocken, PA, USA, 2018.
55. ASTM C469/C469M-14; Standard Test Method for Static Modulus of Elasticity and Poisson's Ratio of Concrete in Compression. ASTM International: West Conshohocken, PA, USA, 2014.
56. ASTM C234; Standard Test Method for Comparing Concretes on the Basis of the Bond Developed with Reinforcing Steel. ASTM International: West Conshohocken, PA, USA, 1991.
57. Meng, L.; Zhang, C.; Wei, J.; Li, L.; Liu, J.; Wang, S.; Ding, Y. Mechanical properties and microstructure of ultra-high strength concrete with lightweight aggregate. *Case Stud. Constr. Mater.* **2023**, *18*, e01745. https://doi.org/10.1016/j.cscm.2022.e01745
58. Bremner, T.W.; Holm, T.A. Elastic compatibility and the behavior of concrete. *ACI J.* **1986**, *83*, 244–250. https://doi.org/10.14359/10422
59. Lu, J.X. Recent advances in high strength lightweight concrete: From development strategies to practical applications. *Constr. Build. Mater.* **2023**, *400*, 132905. https://doi.org/10.1016/j.conbuildmat.2023.132905.
60. Kevinly, C.; Du, P.; Tan, K.H. Local bond-slip behaviour of reinforcing bars in fibre reinforced lightweight aggregate concrete at ambient and elevated temperatures. *Constr. Build. Mater.* **2023**, *377*, 131010. https://doi.org/10.1016/j.conbuildmat.2023.131010
61. Mo, K.H.; Visintin, P.; Alengaram, U.J.; Jumaat, M.Z. Bond stress-slip relationship of oil palm shell lightweight concrete. *Eng Struct* **2016**, *127*, 319–30. https://doi.org/10.1016/j.engstruct.2016.08.064
62. Cairns, J.; Jones, K. An evaluation of the bond-splitting action of ribbed bars. ACI Mater J 1996, 93(1), 10–9. https://doi.org/10.14359/9791
63. Abrishami, H.H.; Mitchell, D. Influence of splitting cracks on tension stiffening. ACI Struct J 1996, 93(6), 703–10.
64. Kadapure, S.A.; Deshannavar, U.B. Bio-smart material in self-healing of concrete. *Materials Today: Proceedings* **2022**, *49*, 1498–1503. https://doi.org/10.1016/j.matpr.2021.07.245
65. Phillips, A.J.; Gerlach, R.; Lauchnor, E.; Mitchell, A.C.; Cunningham, A.B.; Spangler, L. Engineered applications of ureolytic biomineralization: a review. *Biofouling* **2013**, *29*, 715–733. https://doi.org/10.1080/08927014.2013.796550
66. Kim, H.K.; Park, S.J.; Han, J.I.; Lee, H.K. Microbially mediated calcium carbonate precipitation on normal and lightweight concrete. *Constr. Build. Mater.* **2013**, *38*, 1073–1082. https://doi.org/10.1016/j.conbuildmat.2012.07.040
67. Salehi, P.; Dabbagh, H.; Ashengroph, M. Effects of microbial strains on the mechanical and durability properties of lightweight concrete reinforced with polypropylene fiber. *Constr. Build. Mater.* **2022**, *322*, 126519. https://doi.org/10.1016/j.conbuildmat.2022.126519